Catalysis Today 427 (2024) 114410

Contents lists available at ScienceDirect

Catalysis Today

journal homepage: www.elsevier.com/locate/cattod

Assessment of the stability of LTA zeolites under natural gas drying TSA conditions

P.A.S. Moura [a,b], E.D.S. Ferracine [c], E. Rodríguez-Aguado [b], D.A.S. Maia [a], D.C. Melo [d], S. Valencia [e], D. Cardoso [c], F. Rey [e], M. Bastos-Neto [a], E. Rodríguez-Castellón [b,*], D.C.S. Azevedo [a]

[a] Grupo de Pesquisa em Separações por Adsorção, Universidade Federal do Ceará, 60440-900 Fortaleza, CE, Brazil
[b] Departamento de Química Inorgánica, Facultad de Ciencias, Universidad de Málaga, 29071 Malaga, Spain
[c] Laboratório de Catálise, Universidade Federal de São Carlos, 13565–905 Sao Carlos, SP, Brazil
[d] CENPES/Petrobras, Rio de Janeiro, Brazil
[e] Instituto de Tecnología Química, Consejo Superior de Investigaciones Científicas – Universitat Politècnica de València, 46022 Valencia, Spain

ARTICLE INFO

Keywords:
Hydrothermal stability – LTA – Carbon deposition

ABSTRACT

The main features in cationic LTA zeolites that are likely to impact its potential hydrothermal stability are interconnected. The *Al* content and the compensating cation play an important role in the water adsorption but their influence on the zeolite performance in thermal cycles is yet to be understood. In this study, four LTA zeolite samples were synthetized with distinct *Si/Al* ratios in sodium and potassium forms. They underwent a Premature Aging Protocol (PAP) that took into account the operating conditions typically found in temperature swing adsorption processes. The *Si/Al* ratio per se did not impact in the crystallinity upon aging, but the presence of a high amount of potassium cations (*Si/Al* = 1) led to the amorphization of the zeolite structure. The results from XPS and NMR techniques indicate the *Al* migration from the outer surface to the inner cages occurs upon aging. Chemical analysis by XRF and ICP-OES associated with ^{27}Al NMR analysis reveal that the presence of EFAl is particularly significant in the sample with the largest *Si/Al* ratio (5) and is correlated to a much larger *C* deposition upon aging. TG/DTG and TPD-NH_3 experiments suggest that acid sites in the zeolite structures act as a double-edged sword, by enhancing water adsorption while also leading to carbon accumulation. CO_2 isotherms at 0 ºC reveal the reduction of the microporosity after aging, whereas the *Al* content is proportional to the water adsorption uptake, particularly at low pressures (below 10 mbar). The material with an intermediate *Si/Al* ratio and in *Na*-form (LTAc-SiAl2-Na) combines excellent hydrothermal stability with a high-water affinity and uptake.

1. Introduction

The energy requirement keeps increasing steadily worldwide and a diverse energy matrix appears as the key solution to transition towards a decarbonized economy [1,2]. In the last 20 years, the share of Natural Gas (NG) in the global energy matrix has increased more than 2% per year [3]. One of the first unit operations in NG processing is drying in order to avoid problems associated with the hydrate formation, reduction of power efficiency and corrosion and/or erosion of equipment and pipelines [4]. Temperature Swing Adsorption (TSA) has become a mandatory unit operation, following the removal of particulate matter and dew point adjustment [5]. In the adsorption step of a drying TSA cycle, the adsorbent packed in a column is ordinarily submitted to high pressures (around 30 bar) and a gas feed containing CO_2, H_2O and trace heavier hydrocarbons (C5 +), besides methane. Adsorbents to be packed in the TSA column are chosen from hydrophilic materials, such as, zeolites, silicas or aluminas [6].

Zeolites are microporous materials, also known as molecular sieves due to their unique pore size(s) defined by their crystalline structure, which allows smaller molecules (such as water) to be hosted in the internal cages and larger molecules to be excluded. Therefore, this sieving effect may lead to high selectivity. They are composed by tetrahedral units TO_4, *T* being either a silicon or aluminium atom. When the *T* atom is only *Si* (or another tetravalent element), the structure is neutral; however, if it is *Al*, there is a negative charge in AlO_4^-, which must be compensated by a cation (thus generating cationic zeolites) or by a

* Corresponding author.
E-mail address: castellon@uma.es (E. Rodríguez-Castellón).

https://doi.org/10.1016/j.cattod.2023.114410
Received 14 July 2023; Received in revised form 22 September 2023; Accepted 11 October 2023
Available online 17 October 2023

proton (H^+), giving rise to protonic zeolites. The main features in a cationic zeolite that are likely to impact its potential to adsorb water and its hydrothermal stability are interconnected and the *Al* content has a key-role in these features (Fig. 1). The *Al* amount in zeolites is ruled by the Löewenstein law [7] that allows only *Si – O – Al* and *Si – O – Si* bonds, hence the *Si/Al* ratio is never lower than 1.0. Even at room temperature, the *Al* coordination may change between tetrahedral AlO_4, inside the framework, and octahedral, as extra framework *Al*, outside the zeolite structure [8]. The *Al* amount provides local acidity by forming Brönsted sites (bridged hydroxyl) that are composed by a proton (H^+) attracted to a negative framework oxygen, which is linked to an *Al* and a *Si* atom. Nevertheless, cationic zeolites have cations (alkali or earth alkali) to balance the negative charge triggered by the presence of *Al*. The cations content required to balance the charge in the zeolite framework is proportional to the *Al* content and thus enhanced water uptake is also expected. Lewis acid sites are more likely than Bronsted acid sites to occur in cationic zeolites due to structure defects or extra-framework (octahedral) aluminum [9]. Besides water affinity, the widespread use of zeolites in industry comes from their high thermal stability [10]. The thermal resistance comes from the high robustness of *Si – O – Si* bonds, which have pronounced thermal stability, and thus more energy is required to break these bonds as compared to *Al – O – Si* bonds [11,12]. Furthermore, the cation exchange in *Al*-containing zeolites may modify such features.

The main objective of this investigation is to elucidate the effect caused by the *Si/Al* ratio and the compensating cations in the hydrothermal stability of prematurely aged LTA zeolites subject to typical TSA conditions in natural gas drying. Four LTA zeolite samples were synthetized with distinct *Si/Al* ratios (approximately 1, 2 and 5) and submitted to a Premature Aging Protocol (PAP) that emulates the conditions found in real TSA processes for NG drying to probe their hydrothermal stability [13]. A suite of characterization techniques (XPS, XRD, solid state NMR, etc.) indicate that the LTA zeolite adsorbent with an intermediate *Si/Al* ratio (2) and mostly in Na-form (LTAc-SiAl2-Na) combines excellent hydrothermal stability with a high-water affinity and uptake, thus, being a promising adsorbent for this process.

2. Experimental

2.1. Adsorbent syntheses

The synthesis of LTA zeolite with *Si/Al* ratio of approximately 1.0 in *Na* form [10] was performed by dissolving 0.72 g sodium hydroxide in 80 mL H_2O under magnetic stirring for 20 min. Then, 8.26 g sodium aluminate (50–56% Al_2O_3, 37–45% Na_2O) were added to half the volume of the previous solution and 15.48 g sodium metasilicate was added to the other half. Both solutions were stirred by mechanical agitation for 1 h at 27 °C. Then, one solution was added to the other dropwise. The final gel composition was 3.16 Na_2O: 1 Al_2O_3: 1.93 SiO_2: 128 H_2O. The mixture was homogenized by mechanical agitation for 20 min and left to stand in an oven for 4 h (preheated at 100 ºC) to allow the crystals to precipitate. The solids were separated by vacuum filtration, washed with distilled water until the filtrate pH reached neutrality.

LTA zeolite with *Si/Al* ratio approximately 1.0 in *K* form was obtained by ionic exchange replacing the previous sample in *Na* form by *K*. The exchange of *Na* by *K* was carried out according to the following procedure [14]. First, *KCl* was dissolved in deionized water [1 M] and stirred by magnetic agitation for 30 min. Then, *Na*-LTA was added to the salt solution. The suspension was agitated for 24 h followed by the separation of solids by vacuum filtration. This procedure (immersion in *KCl* solution followed by vacuum filtration) was repeated 4 times, always with a freshly prepared salt solution.

The synthesis of LTA zeolite with *Si/Al* ratio of approximately 2.0 in *Na* form [15] starts by diluting 3.08 g sodium aluminate (54% Al_2O_3, 39% Na_2O) in 13.60 g H_2O in a polypropylene bottle under magnetic stirring for 20 min. Then, 28.16 g tetramethyl-ammonium hydroxide (25 wt% in water) were dissolved in 14.66 g H_2O and the solution was stirred magnetically for 20 min. These two previously prepared solutions were mixed and stirred by magnetic agitation for 20 min. Thereafter, 14.80 g Ludox-AS-40 (40 wt% SiO_2) were added and the mixture was stirred for 60 min. The obtained solution was aged in a silicone bath at 27 °C for 24 h. Then, the synthesis gel was left to crystallize in an oven (preheated at 100 ºC) for 28 h inside a polypropylene bottle. The solids were separated by vacuum filtration, washed with distilled water and the filtrate pH was verified until it reached neutrality. The final synthesis gel composition was 1.19 Na_2O: 2.37 $(TMA)_2O$: 1 Al_2O_3: 6 SiO_2: 200 H_2O. The zeolite was calcined at 823 K for 3 hours in air to burn off the occluded organic material.

The synthesis of LTA zeolite with *Si/Al* ratio of approximately 5.0 in *Na* form was prepared as follows [16]. First, 12.00 g tetraethyl-ammonium hydroxide (35 wt%), 11.40 g diethyldimethyl-ammonium hydroxide (20 wt%) and 1.96 g aluminium isopropoxide (98 wt%) were added to a plastic beaker. The mixture was stirred under magnetic agitation for 30 min. Then, 14.20 g Ludox-AS-40 (40 wt% SiO_2) were added to the solution under mechanical agitation for 1 h. The mixture was transferred to a polypropylene bottle and stood in an oven for 24 h (preheated at 373 K) to allow for a pre-crystallization step. Then, after this solution was cooled down, 0.562 g Tetramethyl-ammonium chloride (97 wt%), 0.298 g *NaCl* and 4.03 g water were added. The mixture was stirred for 40 min and transferred to two teflon-lined autoclaves to allow for crystallization in an oven for 3 weeks (preheated at 100 ºC). The solids were separated by vacuum filtration, washed with distilled water and the filtrate pH was verified until it reached neutrality. The final synthesis gel composition was 19.7 SiO_2: 1 Al_2O_3: 6 TEAOH: 4 DEDMAOH: 1 TMACl: 1 NaCl: 342 H_2O. The

Table 1
Summary of the zeolite samples and their labels.

	Material Description			Label	
	Zeolite Structure	*Si/Al* Theoretical	Main Compensating Cation		
1	LTA	1.0	*Na*	LTA_C-SiAl1-Na	(V or A30)
2	LTA	1.0	*K*	LTA_C-SiAl1-K	(V or A30)
3	LTA	2.0	*Na*	LTA_C-SiAl2-Na	(V or A30)
4	LTA	5.0	*Na*	LTA_C-SiAl5-Na	(V or A30)

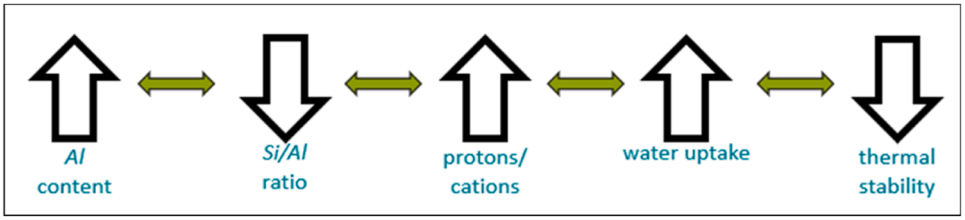

Fig. 1. Interrelation of the main features in zeolites [13].

zeolite was calcined at 550 ºC for 3 hours in air to remove the occluded organic material. All samples and labels are summarized in the Table 1. The labels are complemented with the suffix (V) or (A30), meaning virgin samples and those that underwent the aging protocol, respectively.

2.2. Premature aging protocol – PAP

The Premature Aging Protocol (PAP) emulates the operating conditions that the adsorbent material is subject to in a real TSA process (Fig. 2). Approximately 1.0 g of sample was placed inside the aging chamber and degassed at 10^{-3} mbar for 1 h. Then, a stainless-steel cylinder is connected to the aging chamber, initially containing liquid n-heptane and water (1.0 mL and 0.5 mL, respectively, per gram of sample). n-Heptane was chosen to represent traces hydrocarbons (C5 +) in offshore natural gas plant [17]. The water amount was estimated by the typical water uptake in zeolites [18]. The starting sample was saturated with water and n-heptane vapors by opening valve H and allowing 24 h for adsorption equilibrium to be reached. Subsequently, valve H was closed and the aging chamber was pressurized up to 30 bar total pressure with a CO_2/CH_4 gas mixture (1:4 v/v), by actuating valves F, C and D. After1 hour, the aging chamber was heated up to 573 K (5 K min^{-1}). Then, the sample was left at this temperature and pressure for 30 days.

2.3. Characterization and adsorption techniques

Adsorbent materials were characterized by XRD analyses that were performed in a X´Pert Pro MPD automated diffractometer (PANalytical®). Crystallinity of the zeolites was calculated as the ratio of the area below the main peaks in the 2θ range between 20 and 32º, and that of the pristine (non-aged) sample. XPS spectra, in a Physical Electronic spectrometer (PHI Versa Probe II); XRF analyses, in a UniQuantTM (Thermo Fisher Scientific®); ICP-OES in an Agilent 715-ESTM instrument; SEM analyses in a Magellan® 400 L FEI equipment; DTA/DSC-MS experiments in a TGA/DCS 851e (X-12 Nb), MettlerToledo®; and Elemental Analysis CNH measurements in a Leco TruSpec Micro CHNSO elemental analyzer. TPD-NH_3 experiments were executed as follows: first, 80 mg of adsorbent sample were treated under helium flow (100 mL min^{-1}) and heated up to 620 °C (3 °C min^{-1}). Then, ammonia diluted in *He* flowed through the sample at 100 °C until saturation, which was detected by a mass spectrometer. Lastly, ammonia was desorbed, by switching the flow to *He* and heating the sample up to 800 ºC (10 0 ºC min^{-1}). The porous texture was estimated by adsorption isotherms of CO_2 at 0 ºC , which were measured in an Autosorb iQ3 (Quantachrome Instruments). More information regarding the used characterization techniques are detailed explained in the Supplementary material. Micropore volume was obtained by applying the Dubinin-Radushkevich (DR) equation [19]. Water vapor adsorption isotherms were performed in a high-accuracy gravimetric instrument IGA-002, by Hiden® at 40 ºC and a pressure range up to 70 mbar. Previously, the samples were degassed under vacuum (10^{-5} mbar) at 300 ºC for 10 h. Then, increasing doses of water vapor were added to the sample chamber stepwise and equilibrium was allowed to reach for each injection. Water adsorption experimental data were adjusted using the Aranovich- Donohue Model – ADM (**Eq. 01**) [20]. The model considers both Langmuir-type behavior at low pressures for microporous materials combined with multi-layer adsorption (water clustering) [21,22]. It consists of the product of two terms: the first one represents the Sips Model [23], 'q_{max}' stands for the maximum adsorbed concentration and '*b*' accounts for the adsorbent/adsorbate interaction. As an extension to the Langmuir Model, the Sips Model, takes into account an additional '*n*' parameter, which is related to the degree of heterogeneity of the adsorbent surface. The second term stands for the adsorption at high pressures. It takes into account the saturation pressure "P_0" and an empirical parameter "e" related to the multilayer/clustering adsorption.

$$q_{eq} = \frac{q_{\max} \bullet (b \bullet P)^n}{1 + (b \bullet P)^n} \bullet \frac{1}{1 - \left(\frac{P_0}{P}\right)^e} \quad (1)$$

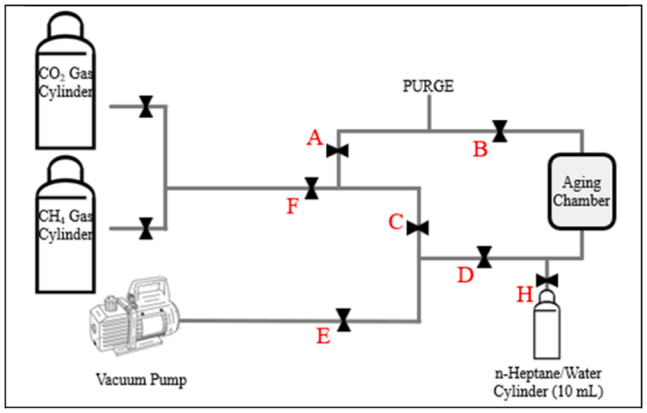

Fig. 2. Premature Aging Protocol (PAP) scheme [13].

3. Results and discussion

Fig. 3 shows the XRD patterns for all pristine and aged LTA materials. The hydrothermal route adopted to synthesize the adsorbents led to well-defined LTA structures, as demonstrated by the comparison with the reference pattern [24]. The main peaks located in the 2θ range from 20° to 32° for *Na*-containing samples with different *Si/Al* ratios (1, 2 and 5) remain in the pristine and aged materials (Fig. 3**(b-d)**). The differences in crystallinity are in the range 1 – 7%, which is marginal (Table 2). On the other hand, the *K* sample (Fig. 3**(a)**) shows a drastic loss of crystallinity (≅ 90%) upon aging (Table 2). Practically all the peaks vanish in the aged *K* sample diffractogram. Together with the drifting of the baseline, this is clear evidence of structure amorphization. It is known that, under continuous thermal treatment, the zeolite structure may transition to a new crystalline phase, which may evolve to an amorphous phase [25]. Previous studies indicate that LTA in potassium form undergoes amorphization at 960 °C, when heated for 0.5 h [25]; there may be re-crystallization into kaliophilite and kalsilite, when heated at temperatures above 1000 °C [26]. In the present study the LTAc-SiAl1-K sample amorphization occurred at a much lower temperature (300 °C), which was maintained for 720 h (Fig. 3**(a)**). Note that zeolites amorphization is also time dependent [27], so it may have happened to sample LTAc-SiAl1-K, despite the relatively low aging temperature. Besides temperature, the presence of large amount of water in the media may also contribute to the amorphization. It is generally accepted that the double four-membered oxygen rings (D4R) are the main responsible building unit for the LTA amorphization due to the reduction of the T – O – T bridges that causes the disruption of the sodalite cages [28]. In the FTIR spectra shown in Fig. 4, the intense band at 558 cm^{-1} (red line) stands for vibrations from the D4R in the pristine materials (LTAc-SiAl1-Na-V and LTAc-SiAl1-K-V) (Fig. 4**(a)** and **(b)**); a decrease in the intensity of this band is verified in the aged K-containing sample (LTAc-SiAl1-K-A30) (Fig. 4**(c)**). The large size of the compensating cation (K^+) and the high density of cations at such low *Si/Al* ratio (=1) is expected to play an important role in the permanent structure deformation. Corroborating the previous statement [29] it must be noted that zeolites with lower *Si/Al* ratios are commonly less thermally stable than those with higher *Si/Al* ratios.

The materials surface composition was analyzed by XPS (Table 3). The carbon content on the surface of pristine materials stands for adventitious carbon, mostly constituted of short chain hydrocarbons species with small amounts of both single and double bound oxygen functionalities [30,31]. In aged samples, the C *1s* contributions may also

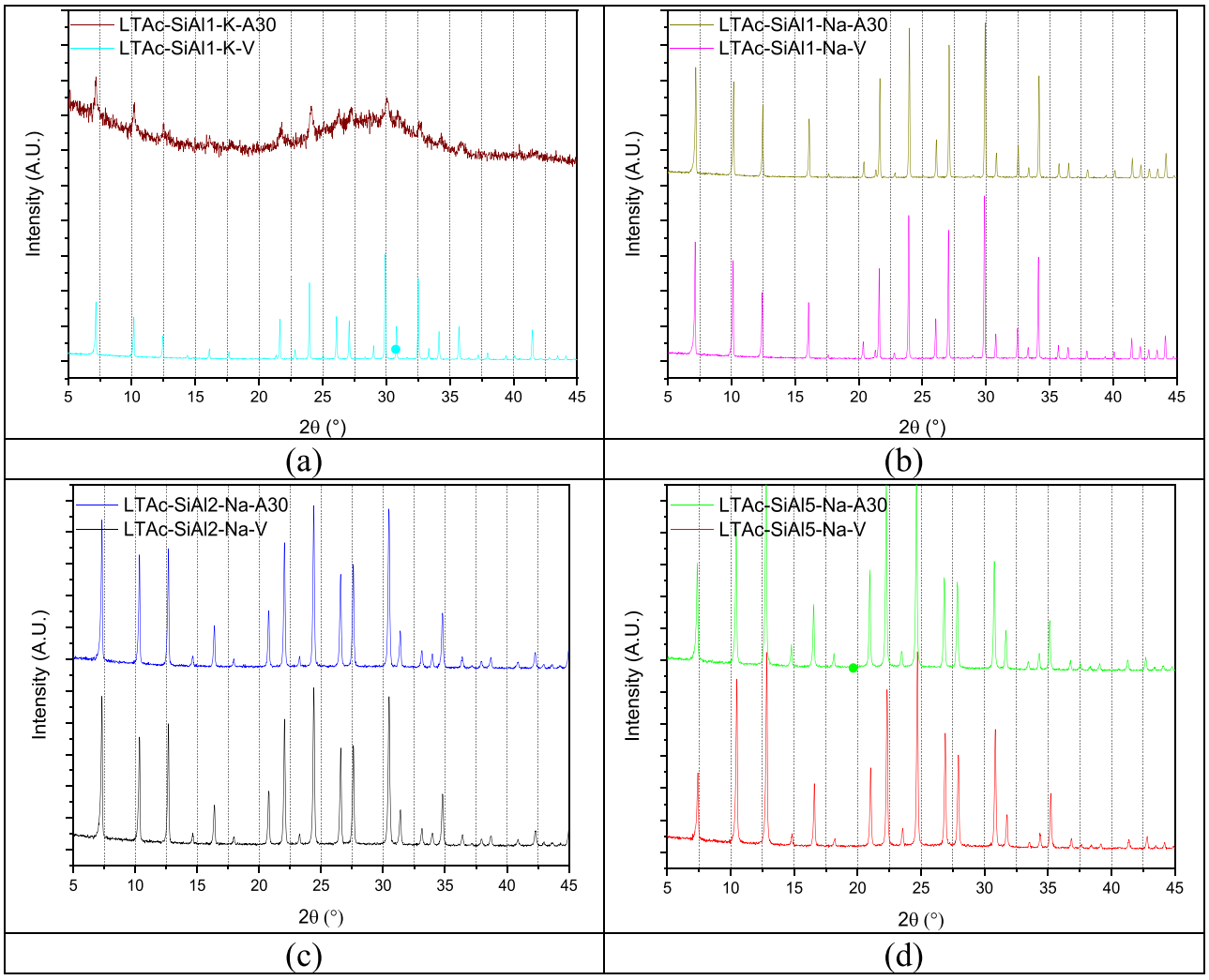

Fig. 3. XRD patterns of LTA_C-SiAl1–K- (V, A30) (a), LTA_C-SiAl1–Na- (V, A30) (b), LTA_C-SiAl2–Na- (V, A30) (c) and LTA_C-SiAl5–Na- (V, A30) (d).

Table 2
Materials crystallinity determined from the XRD patterns of the LTA samples.

Sample	Crystallinity [%]
LTAc-SiAl1-K-V	100
LTAc-SiAl1-K-A30	11
LTAc-SiAl1-Na-V	100
LTAc-SiAl1-Na- A30	93
LTAc-SiAl2-Na-V	100
LTAc-SiAl2-Na- A30	99
LTAc-SiAl5-Na-V	100
LTAc-SiAl5-Na- A30	98

be ascribed to coke formation [32] (Table 4) but, unexpectedly, the relative carbon content is lower after the aging process. These results point out that the formation of carbonaceous deposits (coke) mainly takes place inside the pores of the zeolites, in agreement with elemental analysis (Table 7), which shows a greater amount of carbon content in aged samples. When the *Si/Al* ratio (Table 3) is compared to the carbon content on the surface of aged samples (Table 3), more intense carbon deposition is observed with decreasing *Si/Al* ratio. The *Si/Al* ratio is inversely proportional to the *Al* content and to the cation density on the structure. The contributions from Si 2*p* and Al 2*p* core-level spectra are typical of aluminosilicates and so is O 1 *s* (Table 4) [33,34]. The bulk *Si/Al* ratios agree with those found in the XPS analyses (Table 3 and

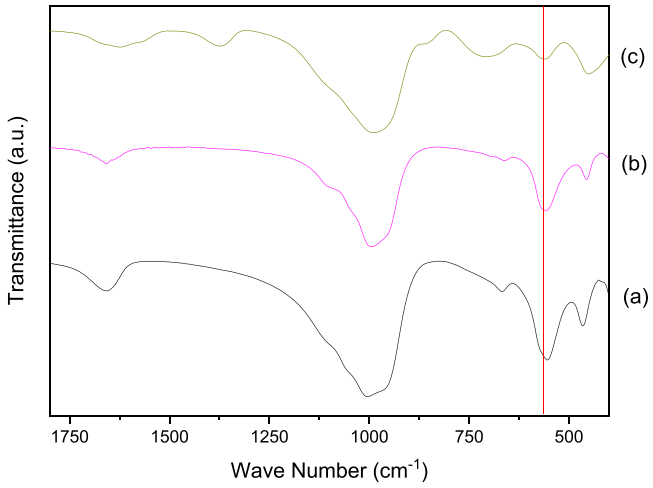

Fig. 4. IR spectra for the LTAc-SiAl1-Na-V (a), LTAc-SiAl1-K-V (b) and LTA_C-SiAl1–K-A30 (c).

Table 5), except for the sample with the highest *Si/Al*. The *Si/Al* ratios found by XPS for the pristine and aged materials suggest that *Al* atoms tend to migrate to the bulk of the solid upon aging.

Bulk chemical compositions of the LTA pristine materials were

Table 3
Chemical surface composition (% atomic concentration) determined by XPS analyses in all LTA samples.

Sample	C 1 *s*	O 1 *s*	Al 2*p*	Si 2*p*	Na 1 *s*	K 2*p*	Si/Al atomic ratio
LTAc-SiAl1-K-V	25.6	43.2	8.9	11.3	-	10.9	1.3
LTAc-SiAl1-K-A30	17.6	50.5	9.9	12.8	-	9.2	1.3
LTAc-SiAl1-Na-V	20.6	46.4	9.9	10.3	12.8	-	1.0
LTAc-SiAl1-Na-A30	10.3	53.5	10.4	12.8	13.0	-	1.2
LTAc-SiAl2-Na-V	18.0	52.7	7.1	16.8	5.5	-	2.4
LTAc-SiAl2-Na-A30	13.6	56.4	7.5	17.7	4.7	-	2.4
LTAc-SiAl5-Na-V	10.0	62.5	3.4	22.7	1.5	-	6.8
LTAc-SiAl5-Na-A30	13.8	59.5	3.0	22.7	1.0	-	7.4

Table 4
Binding energy values (eV) and contributions of all LTA samples.

Sample	Si 2*p*	Al 2*p*	C 1 *s*	O 1 *s*	Na 1*s*	K $2p_{3/2}$
LTAc-SiAl1-K-V	101.5	73.7	284.8	530.6	-	293.2
LTAc-SiAl1-K- A30	102.0	74.1	284.8	531.2	-	293.2
LTAc-SiAl1-Na-V	101.6	73.7	284.9 286.2 288.7	530.8 532.3	1072.0	-
LTAc-SiAl1-Na-A30	101.9	74.0	284.8 286.0	531.2	1072.3	-
LTAc-SiAl2-Na-V	102.7	74.6	284.8 286.5 289.2	531.9	1072.5	-
LTAc-SiAl2-Na-A30	102.7	74.6	284.6 286.0	531.9	1072.5	-
LTAc-SiAl5-Na-V	103.1	74.6	284.6 286.2 288.8	532.4	1072.6	-
LTAc-SiAl5-Na-A30	103.5	75.1	284.9 286.8	532.8	1072.9	-

Table 5
XRF of LTAc-SiAl1- (Na, K) -V and ICP-OES of LTA_C-SiAl (2, 5)– Na– V[*wt%*].

Sample	*Si*	*Al*	*Na*	*K*	*(Na + K) /Al*	*Si/Al* Ratio
LTAc-SiAl1-Na-V	15.9	12.9	15.1	0.0	1.4	1.2
LTAc-SiAl1-K-V	15.8	12.4	0.5	20.0	1.2	1.2
LTAc-SiAl2-Na-V	56.7	28.44	14.8	0.0	0.6	1.9
LTAc-SiAl5-Na-V	81.0	15.98	3.0	0.0	0.2	4.9

obtained by XRF and ICP-OES (Table 5). X-Ray Fluorescence was also used to confirm the ion exchange procedure (*K* in exchange of *Na* ions*)* performed in the LTA sample with the lowest *Si/Al* ratio (~1.0) (Table 5). The analysis showed that nearly 90% cation exchange was achieved (Table 5). Note that the *Si* and *Al* contents obtained from XRF analysis confirm that the *Si/Al* ratio in the bulk is close to 1.00. The carbon deposition upon aging may be affected by the nature of the compensating cations (*Na* and *K*), mainly due to pore accessibility issues posed by the different cation sizes. Furthermore, the cation density and residual acidity (e.g. caused by EFAl) in the framework are also expected to have a role in the carbon deposition [32]. By checking the column *(Na + K)/Al* (Table 5), it is possible to observe that the negative charge generated by *Al* atoms was perfectly balanced in the *K* sample, preventing the formation of strong acid sites. The bulk composition for the samples LTAc-SiAl2-Na-V and LTAc-SiAl5-Na-V was determined by ICP-OES (Table 5). The Si/Al ratios of the samples are in good agreement with those expected, as was also observed from XPS results. By comparing the results for the bulk *Si/Al* ratio (Table 5) obtained either by ICP-OES or XRF to the results found by XPS (Table 3), the *Al* migration from the surface to the inner structure of the solid is corroborated, particularly for the sample with a lower *Al* content (*Si/Al* = 5) [13]. The samples with *Si/Al* greater than 1 show an excess of *Al* atoms as compared to the amount of compensating cations (Table 5) and, therefore, must be counter-balanced by protons or other cationic species. In fact, in the samples LTAc-SiAl5-Na- (V, A30) a fraction of the *Al* amount was identified by ^{27}Al NMR as EFAl (Fig. 5). When this LTA sample is aged, the EFAl content increased, enhancing the general acidity of the material [35]. On the other hand, no EFAl was identified for the sample with an intermediate *Si/Al* ratio (LTAc-SiAl2-Na), which means that excess framework *Al* charge must be neutralized by protons, thus giving rise only to Bronsted acid sites.

^{27}Al and ^{29}Si NMR analyses were performed for all pristine and aged LTA adsorbents (Table 6 and Fig. 5). The presence of EFAl is restricted to the sample with the highest *Si/Al* ratio LTAc-SiAl5-Na- (V, A30) and it increases with the aging. The estimated *Si/Al* ratios obtained from the ^{29}Si NMR spectra (Table 5) remain approximately the same for the pristine and aged samples. Taking into account that *Al* content decreases in some cases on the surface, as indicated by XPS (Table 3), the proposal that *Al* migrates to the inner zeolite structure is plausible [13].

The results of CHN analyses summarized in Table 7 reveal an increasing content of the bulk carbon content upon aging, except for the sample with *Si/Al* = 2. Both samples with the lowest *Si/Al* ratio (LTAc-SiAl1- (Na, K)) present a moderate buildup of *C* when compared to that measured for the sample LTAc-SiAl5-Na. The sample with an intermediate *Si/Al* ratio (LTAc-SiAl2-Na) present the lowest bulk *C* buildup, within the uncertainty of the measurement. In the sample with the highest *Si/Al* ratio, the significant concentration of extra-framework aluminum (Fig. 5) contributes to the general zeolite acidity in the form of Lewis acid sites [35]. These acid sites probably catalyze the reactions of adsorbed hydrocarbons, which find plenty of pore space to be hosted in the zeolite cages (low cation density), thus leading to coke formation [32]. By considering the results from XPS (Table 3) and CHN (Table 7) for this sample, in comparison with the other samples, there is

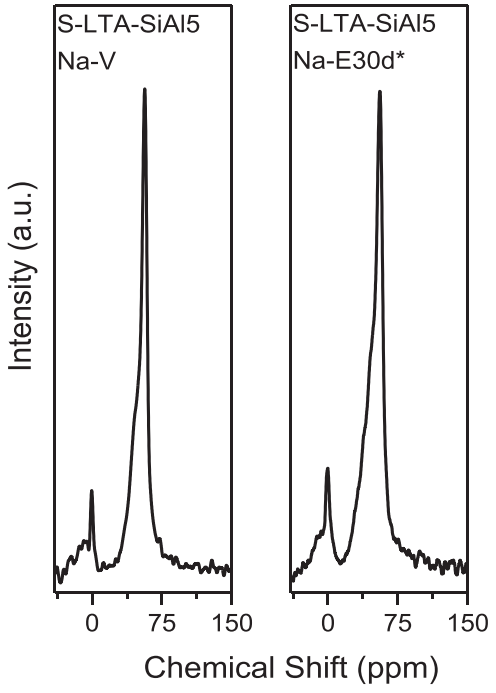

Fig. 5. ^{27}Al NMR spectra of the LTAc-SiAl5-Na- (V, A30).

Table 6
Si/Al ratio obtained from ^{29}Si NMR spectra of all LTA samples.

Sample	Si/Al ratio
LTAc-SiAl1-K-V	1.0
LTAc-SiAl1-K- A30	1.0
LTAc-SiAl1-Na-V	1.0
LTAc-SiAl1-Na- A30	1.0
LTAc-SiAl2-Na-V	2.0
LTAc-SiAl2-Na- A30	2.1
LTAc-SiAl5-Na-V	5.1
LTAc-SiAl5-Na- A30	5.1

Table 7
Carbon content determined by CHN analysis of all LTA samples.

Sample	*C content [%]* Measurement Uncertainty: ± 0.3
LTAc-SiAl1-K-V	< 0.3
LTAc-SiAl1-K- A30	0.9
LTAc-SiAl1-Na-V	< 0.3
LTAc-SiAl1-Na- A30	1.2
LTAc-SiAl2-Na-V	< 0.3
LTAc-SiAl2-Na- A30	0.4
LTAc-SiAl5-Na-V	< 0.3
LTAc-SiAl5-Na- A30	6.9

an evident increase of the carbon content after the aging protocol that suggests that *C* deposition occurs mainly in the inner, but also in the outer material surface. This contradicts the expected trend that samples with higher *Si/Al* ratio would be more stable and less prone to coke deposition. However, it must be taken into account that diffusion at 300 ºC of heptane through LTA windows may be possible. In fact, this trend is observed for the samples with *Si/Al* ratios of 1 and 2 (the latter sample shows negligible coke formation). However, the trend is not confirmed for the sample with high *Si/Al* ratio, very likely due to the presence of extra-framework *Al* acting as a catalyst of coke formation.

The morphology of the crystals was examined by SEM analyses from distinct batches (Fig. 6). Cubic crystals, typical of the LTA structure, are large and well defined for the samples in the *K* and *Na*-forms and *Si/Al* ~1, as shown in Fig. 6 **(a)** and **(b)**, respectively. In contrast, the sample with the highest *Si/Al* ratio (Fig. 6 **(d)**) has much smaller crystals with a poorly defined cubic morphology and tends to form aggregates.

The TG/DTG profiles for all LTA series are shown in Fig. 7. The summary of events is detailed in Table 8, distinguishing between two major mass loss contributions, before and after 300 °C. The main compensating metal (*K*) clearly does not provide a higher stability to the LTA sample with *Si/Al* = 1, which is demonstrated in the nearly flat DTG curve of the aged sample. For the pristine samples containing *Na* at different *Si/Al* ratios (LTAc-SiAl (1, 2, 5)-Na-V), the average mass loss is similar and around 22.6% (Fig. 7). However, the peak (before 300 °C) in the DTG curve is more pronounced and occurs at increasingly higher temperatures for decreasing *Si/Al* ratios, which suggests a higher affinity between adsorbed species (water vapor and atmospheric gases) and zeolite frameworks with higher *Al* content. Regarding aged materials, the samples with the lowest (LTAc-SiAl1-Na-A30) and the highest (S-LTAc-SiAl5-Na-A30) *Si/Al* ratios show significant mass losses above 300 °C (Table 8), which is evident from the peaks shown in the DTG curves in this temperature range. In the sample with *Si/Al* = 5, acid sites are likely to be present in the structure, as suggested by the unbalance between *Na* and *Al* atoms (Table 5) and a considerable amount of EFAl detected by NMR. The higher carbon deposition (Table 7) agrees with the hypothesis of Lewis acid sites due to EFAl [35–37]. In turn, the sample with *Si/Al* = 1 also has a considerable mass loss above 300 °C, but less pronounced than that for sample with *Si/Al* = 5 and occurring at a lower temperature (below 400 °C). Actually, the DTG curve of the pristine sample (LTAc-SiAl1-Na-V) also shows a shoulder in the same temperature range. Therefore, the carbon deposit observed for this sample is probably due to the strong polarity brought about by a high density of *Al* and compensating cations in the structure. The strongly bound water may give rise to (Bronsted) acid sites that trigger the polymerization of n-heptane leading to "softer" coke than that formed in the sample with *Si/Al* = 5. The sample LTAc-SiAl2-Na-V also presents an unbalanced charge (Table 5), or excess *Al* in the framework. Nevertheless, negligible carbon deposition (Table 7) is observed, resulting in a modest mass loss above 300 °C (Table 8). Although there is excess *Al* in the structure, the density of cations is half that of the sample with *Si/Al*= 1 and no EFAl is present, all of these providing the sample LTAc-SiAl2 the highest stability among all samples studied.

From the TPD-NH_3 analyses (Fig. 8), it is possible to assess the total acidity of the samples. With no exceptions, the materials release the majority of NH_3 amount at temperatures below 300 °C, indicating that it was predominantly physisorbed at the surface. In addition, all samples present a decrease in desorbed ammonia between pristine and aged materials, which can be explained by the carbon deposition of aged materials that obstruct the access of NH_3 molecules to the available adsorption sites in zeolites surfaces. As expected, the potassium sample has a smaller desorbed NH_3 amount than the sodium samples, due to the size of the compensating cation (*K*) that fills the available pore volume in the structure and the partial amorphization of the aged sample (Fig. 3). The outcomes from NH_3 desorption (Fig. 8) corroborate with TG/DTG results (Fig. 7 and Table 8) for the *K* samples, the amorphized structure did not allow the NH_3 to be appreciably adsorbed. Regarding the samples LTAc-SiAl1-Na- (V, A30), the aged material undergoes a great reduction in the desorbed NH_3 under 300 °C that corroborate with the intermediate *C* deposition (Table 7). On the other hand, at temperatures above 300 °C, basically no reduction was observed in the desorption quantity. The samples LTAc-SiAl2-Na- (V, A30) had a moderate reduction in the desorbed amount below 300 °C that is explained by the carbon deposition triggered by the aging protocol. Focusing on the region above 300 °C, it is possible to note that stronger acid sites were present in the pristine material that corroborate with the unbalanced charge of *Al* (Table 5) and the absence of EFAL. However, the aging protocol causes the inaccessibility to acid sites, due to the *C* deposition and, thus, intermediate reduction of the NH_3 desorbed above 300 °C can be observed. No particular modifications were identified by TG/DTG analysis (Fig. 7), confirmed by the TPD-NH_3 analysis (Fig. 8) that show the increasing *C* deposition and decreasing NH_3 desorbed as a result of the aging protocol. The samples LTAc-SiAl5-Na- (V, A30) present a decreasing in NH_3 desorbed mainly in the region that is governed by acid sites (above 300 °C), by means of Lewis acid sites, possibly produced by the EFAl species that retain NH_3 adsorbed on the surface up to higher temperatures. In addition, the highest carbon deposition over the aging protocol (Table 7) causes a sharp decrease in the desorbed ammonia for the aged sample as compared to the pristine one. From TG/DT analyses (Table 8), the mass fraction lost over 300 °C increases in more than 30%, however NH_3 desorbed decreases (Fig. 8) in the same temperature range, hence the carbon deposits preferentially occur in acid sites produced by the presence of EFAl in this material.

From CO_2 isotherms at 273 K for all pristine and aged LTA samples (Fig. 9), it is possible to see that the *Si/Al* ratio and the main compensating cations have an impact on the porous texture of the samples. The same group of isotherms is presented in linear (Fig. 9**(a)**) and logarithmic scales (Fig. 9**(b)**), the latter highlighting the low-pressure range. The abrupt rise presented by the isotherms up to a relative pressure of 0.01 indicates a strong adsorbent-adsorbate interaction. It is important to take in account that CO_2 gas has a quadrupole momentum that may impact in the total porosity. Besides that, it may form geminal complexes that affect the molecules accessibility to the pores. On the other hand, CO_2 molecules showed an interesting capacity in measure microporosity in that low pressure range, also due to its ability to overcome diffusivity barriers, when it is surrounded by cryogenic temperatures [38].

The higher the content of *Al* is, the higher uptake is observed at low

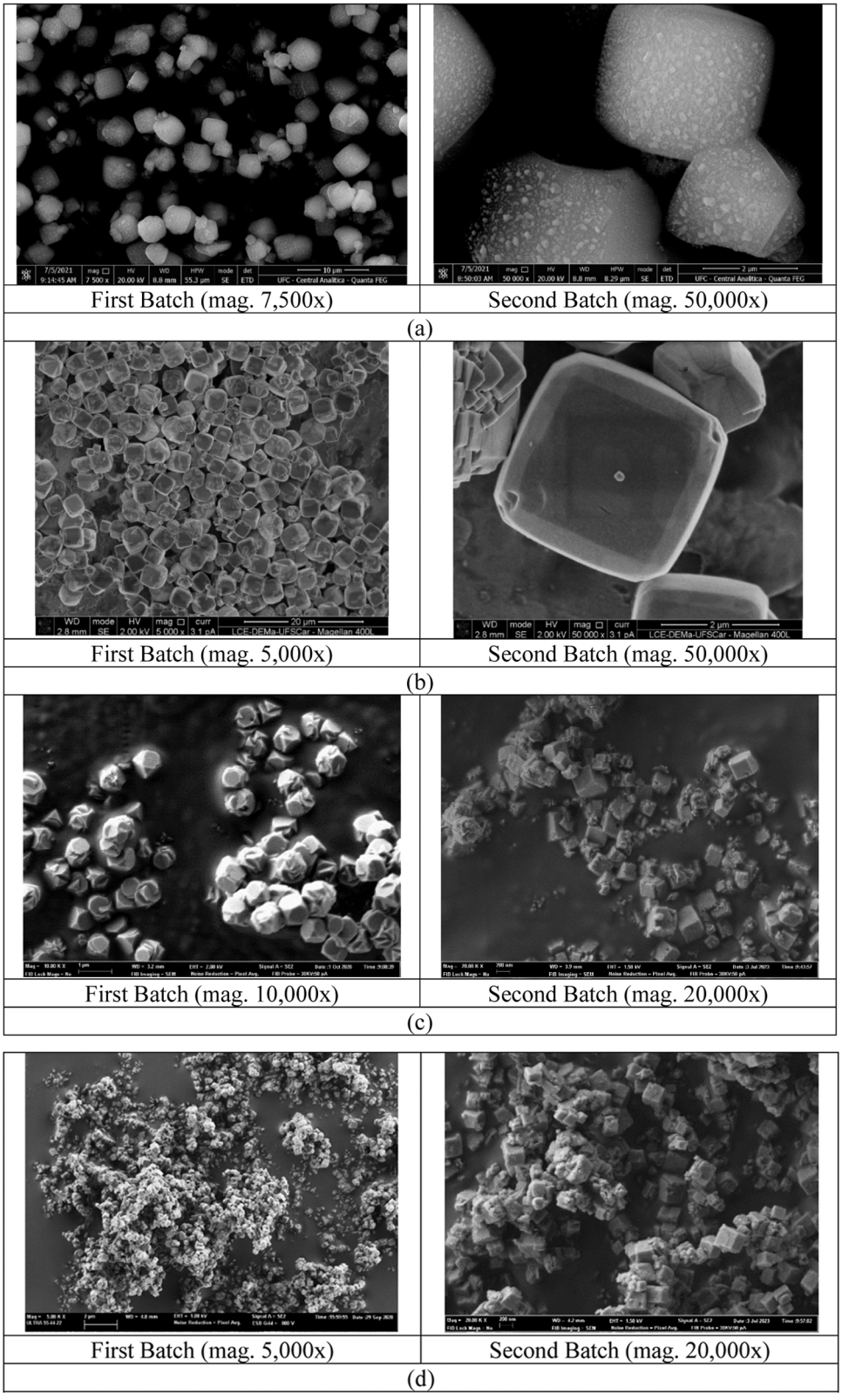

Fig. 6. SEM images of LTAc-SiAl1-K-V (a), LTAc-SiAl1-Na-V (b), LTAc-SiAl2-Na-V (c) and LTAc-SiAl5-Na-V (d).

pressures (Fig. 9**(b)**). This high adsorbate/adsorbent affinity may be explained by the high cations density, which enhances the affinity for CO_2 molecules. After $P/Po = 10^{-3}$, in LTAc-SiAl(1, 2)-Na-(V, A30) samples, the adsorption uptake is majorly dictated by the available pore volume in the zeolitic structures, which is higher for samples with lower density of cations. For pristine zeolites, at sufficiently high pressures, the uptake of the *Na* sample with $Si/Al = 2$ surpasses that of the sample with $Si/Al = 1$ and an analogous trend is expected for the pristine sample with $Si/Al = 5$, if its isotherm could be extrapolated. The CO_2 isotherms for the aged sample with an intermediate Si/Al ratio (~2) does not differ

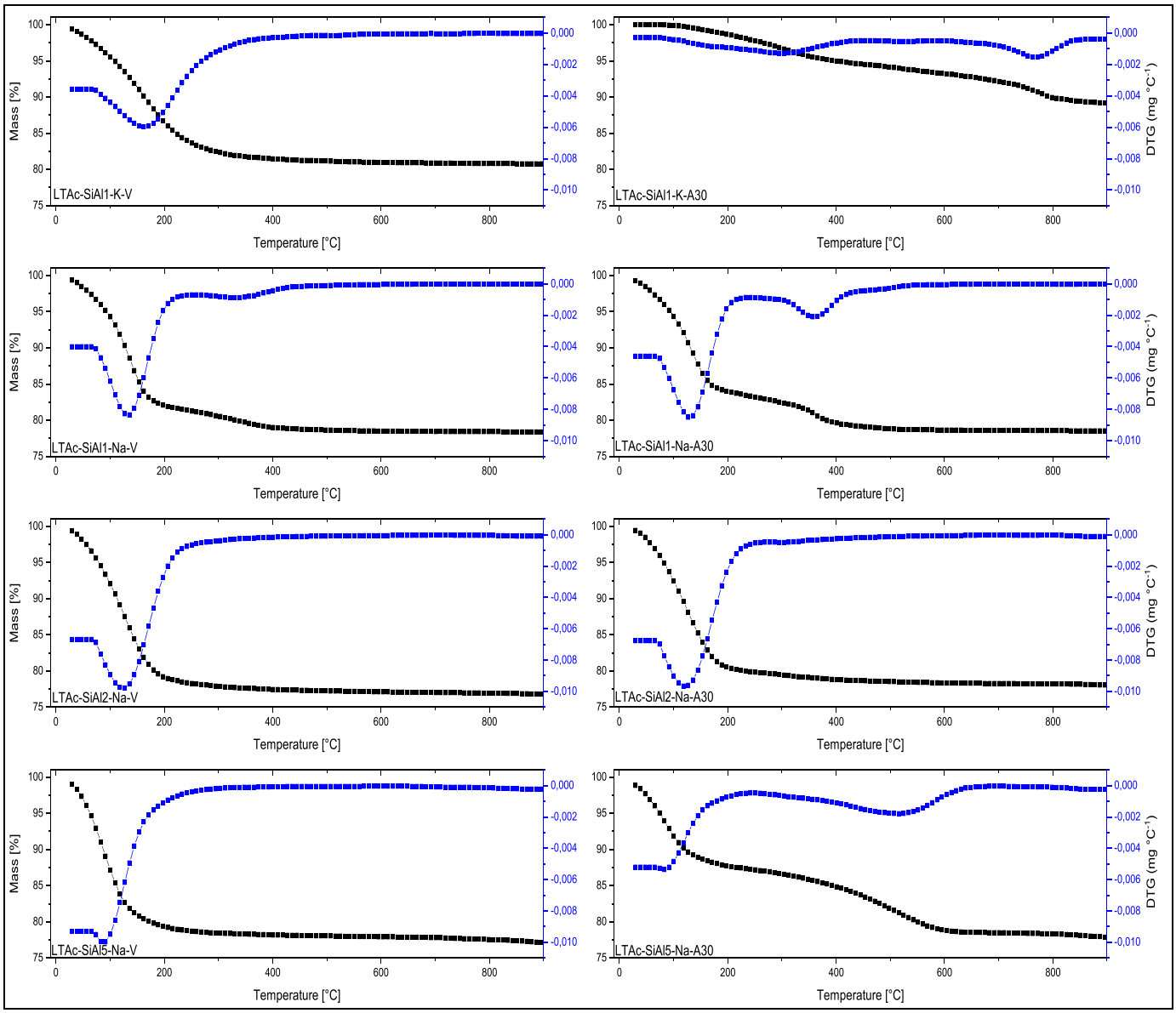

Fig. 7. TG/DTG curves of all LTA samples.

Table 8
Results obtained from thermal experiments (TG/DTG) of all LTA samples.

Sample	Mass Loss [%]	Temperature [°C]	Mass Loss Fraction [%]
LTAc-SiAl1-K-V	19.2	Under 300 °C	91.7
		Above 300 °C	8.3
LTAc-SiAl1-K-A30	11.0	Under 300 °C	30.0
		Above 300 °C	70.0
LTAc-SiAl1-Na-V	21.7	Under 300 °C	89.4
		Above 300 °C	10.6
LTAc-SiAl1-Na-A30	21.5	Under 300 °C	81.9
		Above 300 °C	18.1
LTAc-SiAl2-Na-V	23.2	Under 300 °C	95.2
		Above 300 °C	4.8
LTAc-SiAl2-Na-A30	22.0	Under 300 °C	93.6
		Above 300 °C	6.4
LTAc-SiAl5-Na-V	22.9	Under 300 °C	94.3
		Above 300 °C	5.7
LTAc-SiAl5-Na-A30	22.1	Under 300 °C	60.6
		Above 300 °C	39.4

considerably as compared to the pristine sample (Fig. 9, Table 9). This result is corroborated by the lowest *C* deposition between all aged materials (Table 7) and the very similar TG/DTG curves between pristine and aged samples. The sample with a high *Si/Al* ratio (LTAc-SiAl5-Na) presents a modest adsorption capacity at low relative pressures (up to 10^{-3}), which agrees with the low *Al* content in the structure and hence much less polar framework. At relative pressures above 10^{-3}, the increase in adsorbed concentration presented by the LTAc-SiAl5-Na-V is much steeper than any other LTA material, which is better seen in the log scale (Fig. 9**(b)**). The maximum adsorbed amount reaches the same level of the LTAc-SiAl1-Na-V sample (Table 9), with a trend to go beyond as a consequence of possibly much larger pore space in this sample due to the low cation density. In the pristine and aged *Na* sample with *Si/Al* = 5 (Fig. 9**(a)**), isotherms are much less steep in comparison to other similar materials. The rectangular character of the isotherms is proportional to the adsorbent/adsorbate affinity; hence a lower affinity is confirmed for this sample containing less *Al*. The aged sample (LTAc-SiAl5-Na-A30) shows the lowest adsorption capacity of all *Na*-containing samples, mainly due to the highest carbon deposition (Table 7) whose formation is likely to be related to the EFAl presence. The larger

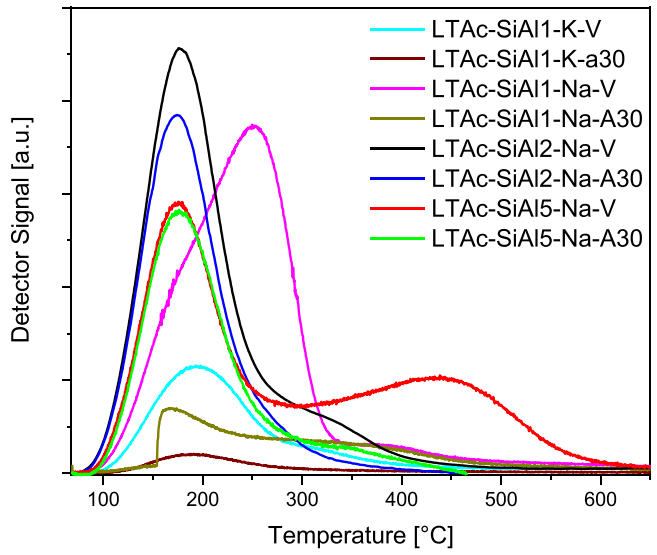

Fig. 8. Detector signal in NH_3 Temperature-Programmed Desorption measurements of all LTA samples.

cation size of *K* and its high density in the sample with *Si/Al* = 1 have partially collapsed the zeolite structure (Fig. 3) which, associated with the *C* deposition (Table 7), causes a drastic drop in CO_2 adsorbed amount (Fig. 9), leading to an uptake reduction of approximately 90% (Table 9).

To measure the accessible micropore volume, the Dubinin-Radushkevich equation [19] was applied to CO_2 isotherms at 0 °C [39] (Fig. 9) and the results are summarized on Table 9. The sample in *Na*-form with a *Si/Al* ratio of 1 presents a moderate decrease in the micropore volume from pristine to the aged material, approximately 15%. Possibly the high *Al* content (Table 5), enhances the acidity, this in turn, favors de coke deposition (Table 7) that obstruct the pores [32]. The porosity of the sample LTAc-SiAl2-Na exhibits the lowest decrease in micropore volume upon aging (Table 8), which is corroborated by the lowest *C* deposition (Table 7). As expected, the pristine sample LTAc-SiAl5-Na-V has the highest micropore volume but it undergoes the sharpest decrease of all *Na*-samples upon aging (Table 9), prompted by the *C* deposition (Table 7) associated with the excess *Al* in the form of EFAl. Concerning the *K*-containing sample (LTAc-SiAl1-K), the pristine material already has a small micropore volume, mainly due to the large compensating cation size (K^+).

Water vapor adsorption isotherms at 40 °C were measured for all LTA samples in a pressure range up to 70 mbar (Fig. 10). The high adsorbent/adsorbate interaction is demonstrated by the sharp rise in adsorbed concentration in all materials, except for the aged *K*-containing sample. H_2O molecules are incorporated in the framework of the cationic zeolites by two different ways: (1) extra-framework compensating cations are surrounded by oxygen atoms of the framework, which contributes to negative electric charges, generating strong interactions with water; associated with the hydration of the extra-framework cations [41,42]; and (2) by weak bonds with the zeolite, upon pore/channel filling [43]. In the pressure range up to 10 mbar, for *Na*-containing samples, the *Al* content is proportional to the framework polarity and hence its hydrophilicity, i.e., the sample with *Si/Al* = 1 shows the highest H_2O uptakes, followed by that with *Si/Al* = 2 and that with *Si/Al* = 5. The attraction for water molecules in cationic zeolites is driven by a dipole-field interaction [44]. The different electronegativity presented by *H* and *O* in water molecules, makes *O* atom work as a Brönsted Acid Site (BAS). In contrast, the tetrahedral *Al* in the zeolites Primary Building Unit (PBUs) works as a Brönsted Basic Site, thus providing an acid and base interaction. Beyond 10 mbar, the low (1) and intermediate (2) *Si/Al* ratio samples reach a plateau on the adsorbed concentration, which is roughly constant in the range from 10 to 50 mbar. Above 50 mbar, the higher availability of larger pore volume of the *Na*-sample with *Si/Al* = 5 allows for a continuous increase in water uptake showed by the rising adsorption close to the water saturation pressure. The sample containing *K* has a considerably lower uptake as compared to the *Na* sample of the same *Si/Al* ratio due to the larger size of the potassium cation. Following

Table 9
Adsorption capacity and micropore volume obtained by CO_2 isotherms of all LTA samples.

Samples	Maximum Adsorption Capacity* [$cm^3\ g^{-1}$]	Micropore Volume [$cm^3\ g^{-1}$]
LTAc-SiAl1-K-V	33.5	0.086
LTAc-SiAl1-K-A30	2.7	0.005
LTAc-SiAl1-Na-V	112.9	0.240
LTAc-SiAl1-Na-A30	75.1	0.202
LTAc-SiAl2-Na-V	127.0	0.309
LTAc-SiAl2-Na-A30	124.5	0.278
LTAc-SiAl5-Na-V	110.9	0.330
LTAc-SiAl5-Na-A30	61.3	0.208

References: [19,40]
* At a relative pressure of 0.029

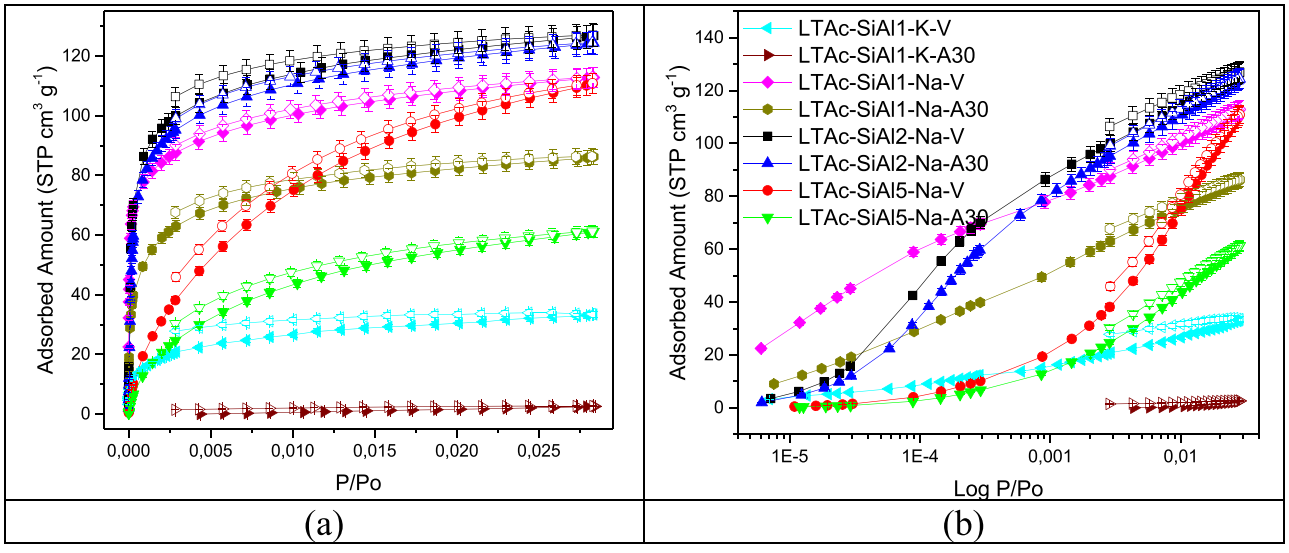

Fig. 9. CO_2 isotherms at 273 K in linear (a) and logarithmic (b) scales of all LTA samples.

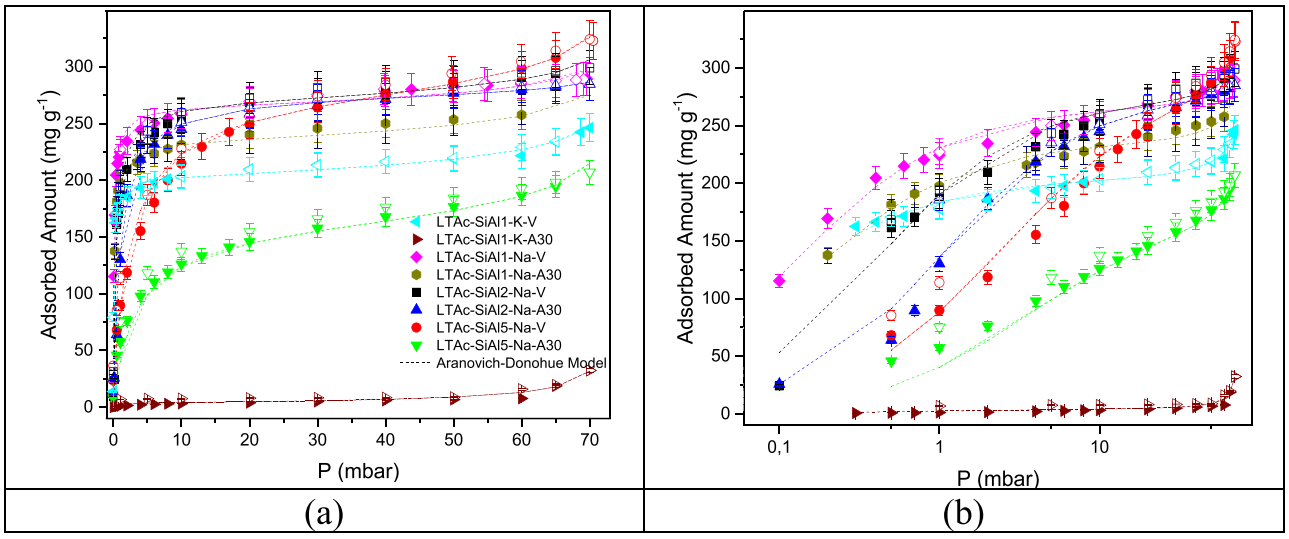

Fig. 10. H_2O isotherms at 313 K in linear (a) and logarithmic (b) scales of all LTA samples.

the previous discussion for the aged *K*-sample, water uptake is also marginal. The XRD pattern clearly indicated the framework collapse due to the rupture of D4R rings (Fig. 3e **4**), which had already been reported by Kosanović et al., 1997 [25].

Regarding the *Na*-containing samples, the one with intermediate (2) *Si/Al* ratio was less affected by aging than the sample with a low *Si/Al* ratio (1) (Table 10), which is more evident in the range from 10 to 50 bar. In fact, Cruciani, 2006 states that *Si* forms a more stable bond with the *O* atom than *Al*, which enhances the hydrothermal stability. Therefore, the aging protocol, at least under the present conditions, did not lead to a considerable decrease in water adsorption for the sample with *Si/Al* = 2 (Fig. 10). It would be expected that the sample with the highest *Si/Al* ratio (5) would be even more resistant to aging because of its much more neutral framework. Nevertheless, it is the one *Na*-containing samples with the highest drop in water uptake upon aging. As previously discussed, this is also the sample with the largest fraction of *Al* present outside the framework (Fig. 5). EFAl provides Lewis acid sites that probably catalyzed coke formation, suggested by the carbon deposition (Table 7) and decrease in textural properties (Table 9).

Experimental adsorption data **(**Fig. 10**)** were adjusted by the AD model, which theoretically estimates the contribution from the monolayer (or adsorption in the crystalline framework) and subsequent layers (or adsorption in larger pores due to crystal defects or interstitial voids). The model parameters are summarized in Table 11. The parameter that accounts for the maximum adsorption uptake (q_{max}) is mainly influenced by the accessible pore volume. Hence, the sample LTA-SiAl5-Na-V - with the highest pore volume, associated with the low cation density - has the highest (q_{max}) value (Table 11). On the other hand, the sample with a low *Si/Al* ratio (i.e., a high content of compensating cation) and a large cation size, LTAc-SiAl1-K, has the smallest available pore volume

Table 10
Water vapor adsorption capacity at 0.1, 1, 10 and 70 mbar of all LTA samples.

Sample		$H_2O_{(v)}$ Adsorption Capacity [mmol g^{-1}]			
		0.1 mbar	1.0 mbar	10.0 mbar	70.0 mbar
LTAc-SiAl1-K	V	6.17	10.21	11.23	13.75
	A30	0.04	0.13	0.23	1.76
LTAc-SiAl1-Na	V	6.61	12.80	14.55	16.50
	A30	5.54	11.14	12.85	15.27*
LTAc-SiAl2-Na	V	2.95	10.57	14.47	17.00
	A30	1.36	7.55	13.92	15.93
LTAc-SiAl5-Na	V	0.83*	4.89	12.40	18.27
	A30	0.33*	2.24	6.88	11.93

* Estimated from the Aranovich-Donohue model

Table 11
Parameters obtained in Aranovich-Donohue model fittings of H_2O isotherms at 313 K of the LTA samples.

Sample	Parameters			
	q_{max} [mg g^{-1}]	b [$mbar^{-1}$]	n	e
LTAc-SiAl1-K-V	202.79	12.36	0.90	0.07
LTAc-SiAl1-K-A30	4.15	1.38	0.80	0.70
LTAc-SiAl1-Na-V	265.30	7.98	0.91	0.04
LTAc-SiAl1-Na-A30	234.48	7.17	0.90	0.06
LTAc-SiAl2-Na-V	270.13	2.41	0.99	0.04
LTAc-SiAl2-Na-A30	275.01	0.97	0.98	0.02
LTAc-SiAl5-Na-V	281.05	0.42	0.91	0.06
LTAc-SiAl5-Na-A30	165.32	0.30	0.90	0.11

and thus, the smallest (q_{max}) parameter. The impact of aging in the *K* sample, LTAc-SiAl1-K-A30, reduces even more the (q_{max}) parameter (Table 11). The parameter (*b*) is related to the adsorbent/adsorbate interaction; it consistently decreases in magnitude for the aged samples as compared to the pristine counterparts. Concerning the non-aged materials, the LTAc-SiAl1-Na-V sample has the highest value of *b* parameter (7.98) (Table 11), which is consistent with its sharpest rise in the adsorption isotherm in the low-pressure zone (Fig. 10). The homogeneity of adsorption sites is qualitatively assessed by the parameter (*n*), which is reduced in all cases after aging, though very modestly for the *Na* samples with low and intermediate *Si/Al* (Table 11). Lastly, the (*e*) parameter is related to the clustering and condensation of water molecules in larger voids, regarding those pores in the micropore range. The closer (*e*) gets to unity, the more intense will be the rise in uptake close to the saturation pressure. For the samples under study, all (*e*) values are relatively small, except for the aged *K* sample and the aged *Na* sample with the largest *Si/Al* (=5).

4. Conclusions

In order to assess water adsorption and hydrothermal stability, LTA samples were synthesized with three different *Si/Al* ratios (1, 2 and 5), one of them containing two types of compensating cations (*Na, K*). The aging protocol caused a moderate to intense degradation in LTA adsorbents, which was found to be related to the framework polarity, extra-framework *Al* and cation size. The *Si/Al* ratio per se did not impact in the crystallinity upon aging, but the presence of a high density of potassium (in sample of *Si/Al* = 1) led to the amorphization of the zeolite structure. The results from XPS and NMR techniques indicate that

Al migration from the outer surface to the inner cages is occurring with aging. Chemical analysis by XRF and ICP-OES associated with ^{27}Al NMR analysis reveal that the presence of EFAl is particularly significant in the sample with the largest *Si/Al* ratio and is correlated to a much larger *C* deposition upon aging. Contrary to what would be expected for a nearly apolar framework, the aged *Na* sample with *Si/Al* = 5 had the most drastically affected textural features, such as, the available micropore volume, identified by the CO_2 isotherms at 0 ºC. TG/DTG related to TPD-NH_3 experiments showed acid sites in the zeolite structures intensify the water adsorption but also the *C* deposition. In addition, SEM images showed the evolution of the classical cubic morphology of LTA crystals into clusters/aggregates as the *Si/Al* ratio increases, accompanied by a decrease in the crystal size. Likewise, these findings were reflected in the water adsorption isotherms of pristine and aged samples. The *Al* content resulted to be proportional to the water adsorption uptake, particularly at low pressures (below 10 mbar). The samples with an intermediate (2) and low (1) *Si/Al* ratios presented a high affinity for water molecules, giving rise to very rectangular-shaped isotherm. The material with an intermediate *Si/Al* ratio and in Na-form (LTAc-SiAl2-Na) combines excellent hydrothermal stability and high-water affinity and uptake. Though most commercial LTA zeolites that are recommended for gas drying have *Si/Al* = 1, for prolonged TSA operation in the presence of trace hydrocarbons, the sodium LTA sample with *Si/Al* = 2 seems to be the best choice.

CRediT authorship contribution statement

Pedro Augusto S. Moura: Investigation-experimental work, Writing – original draft, Validation. **E.D.S. Ferracina:** Investigation-experimental work; measurements. **E. Rodríguez-Aguado:** Investigation-experimental work. D.A.A. Maia: Investigation; experimental work; validation. **D.C. Melo:** Experimental work. S. Valencia: Conceptualization; Validation; Supervision. D. Cardoso: Conceptualization; Supervision. **F. Rey:** Conceptualization; Validation; Supervision; Writing. **M. Bastos-Neto:** Validation; Supervision. **Enrique Rodríguez-Castellón:** Investigation; Validation; Supervision; Writing; Funding acquisition and Editing. Diana. C.S. Azevedo: Conceptualization; Investigation; Validation; Supervision; Writing; Funding acquisition and Editing.

Declaration of Competing Interest

The authors declare that they have no known competing financial interests or personal relationships that could have appeared to influence the work reported in this paper.

Data Availability

No data was used for the research described in the article.

Acknowledgements

The authors acknowledge financial support from Petrobras (Brazil) project 2018/00130-5, *CAPES* (Brazil), particularly in the frame of project CAPES/Print 88887.311867/2018–00 and *Servicios Centrales de Apoyo a la Investigación – SCAI*. S.V. and F. R. acknowledge financial support by the Spanish Ministry of Science and Innovation (CEX2021-001230-S grant funded by MCIN/AEI/10.13039/ 501100011033 and TED2021–130191B-C41 and TED2021-130756B-C31 grants funded by MCIN/AEI/10.13039/501100011033 and by "ERDF A way of making Europe" by the European Union NextGenerationEU/PRTR). Authors thank also the financial support by the Generalitat Valenciana (Prometeo 2021/077). This study forms part of the Advanced Materials programme and was supported by MCIN with partial funding from European Union Next Generation EU (PRTR-C17. I1) and by Generalitat Valenciana (MFA/2022/047 and MFA/2022/012).

Appendix A. Supporting information

Supplementary data associated with this article can be found in the online version at doi:10.1016/j.cattod.2023.114410.

References

[1] B.P. BPSTATS, Statistical Review of World Energy Statistical Review of World. The Editor BP Statistical Review of World Energy, 68th edition.,, 2019, pp. 1–69. ⟨https://www.bp.com/content/dam/bp/business-sites/en/global/corporate/pdfs/energy-economics/statistical-review/bp-stats-review-2019-full-report.pdf⟩.
[2] VGB, VGB Powertech Report 2019|2020, 2020.
[3] OECD, Monthly Gas Statistics (Dec/2019), 2020.
[4] H. Rezvani, S. Fatemi, Influence of water vapor condensation inside nano-porous 4A adsorbent in adsorption-desorption cyclic process of natural gas dehydration, Sep. Sci. Technol. (Phila.) 55 (2020) 1286–1302, https://doi.org/10.1080/01496395.2019.1593455.
[5] M.G.R.S. Santos, L.M.S. Correia, J.L. de Medeiros, O. de, Q.F. Araújo, Natural gas dehydration by molecular sieve in offshore plants: Impact of increasing carbon dioxide content, Energy Convers. Manag 149 (2017) 760–773, https://doi.org/10.1016/j.enconman.2017.03.005.
[6] M. Bastos-Neto, D.C.S. Azevedo, S.M.P. Lucena, Adsorption, in: Kirk-Othmer Encyclopedia of Chemical Technology, Wiley, 2020, pp. 1–59, https://doi.org/10.1002/0471238961.0104191518212008.a01.pub3.
[7] W. Loewenstein, The distribution of aluminum in the tetrahedra of silicates and aluminates, Am. Mineral. 39 (1954) 92–96.
[8] B. Xu, F. Rotunno, S. Bordiga, R. Prins, J. Vanbokhoven, Reversibility of structural collapse in zeolite Y: alkane cracking and characterization, J. Catal. 241 (2006) 66–73, https://doi.org/10.1016/j.jcat.2006.04.009.
[9] M. Ravi, V.L. Sushkevich, J.A. van Bokhoven, Towards a better understanding of Lewis acidic aluminium in zeolites, Nat. Mater. 19 (2020) 1047–1056, https://doi.org/10.1038/s41563-020-0751-3.
[10] S. Mintova, N. Barrier, Verified Syntheses of Zeolitic Materials, Third Ed., International Zeolite Association - IZA, Caen - FR, 2016.
[11] G. Cruciani, Zeolites upon heating: Factors governing their thermal stability and structural changes, J. Phys. Chem. Solids 67 (2006) 1973–1994, https://doi.org/10.1016/j.jpcs.2006.05.057.
[12] G.T. Kerr, Intracrystalline rearrangement of constitutive water in hydrogen zeolite Y, J. Phys. Chem. 71 (1967) 4155–4156, https://doi.org/10.1021/j100871a079.
[13] P.A.S. Moura, E. Rodríguez-Aguado, D.A.S. Maia, D.C. Melo, R. Singh, S. Valencia, P.A. Webley, F. Rey, M. Bastos-Neto, E. Rodríguez-Castellón, D.C.S. Azevedo, Water adsorption and hydrothermal stability of CHA zeolites with different Si/Al ratios and compensating cations, Catal. Today (2021), https://doi.org/10.1016/j.cattod.2021.11.042.
[14] P.A.S. Moura, D.P. Bezerra, E. Vilarrasa-Garcia, M. Bastos-Neto, D.C.S. Azevedo, Adsorption equilibria of CO_2 and CH4 in cation-exchanged zeolites 13X, Adsorption 22 (2016) 71–80, https://doi.org/10.1007/s10450-015-9738-9.
[15] R.L. Wadlinger, E.J. Rosinski, C.J. Plank, Synth. Zeolite 3 (375) (1968) 205.
[16] J.G. Moscoso, G.J. Lewis, Crystalline Aluminpsilicate Zeolitic Composition: UZM-9, WO 03/068679 A1 (2003).
[17] R. Gomes Santiago, B. Ferreira dos Santos, I. Gomes Lima, K. Oliveira Moura, D. Carrijo Melo, W. Mantovani Grava, M. Bastos-Neto, S.M. Pereira de Lucena, D. Cristina Silva de Azevedo, Investigation of premature aging of zeolites used in the drying of gas streams, Chem. Eng. Commun. 206 (2019) 1378–1385, https://doi.org/10.1080/00986445.2018.1533468.
[18] Y. Wang, Measurements and Modeling of Water Adsorption Isotherms of Zeolite Linde-Type A Crystals, Ind. Eng. Chem. Res 59 (2020) 8304–8314, https://doi.org/10.1021/acs.iecr.9b06891.
[19] L.V. Dubinin, M.M., Radushkevich, Equation of the characteristic curve of activated charcoal, Proc. Acad. Sci. Phys. Chem. Sec. USSR. 55 (1947) 331–333.
[20] G.L. Aranovich, M.D. Donohue, A new approach to analysis of multilayer adsorption, J. Colloid Interface Sci. 173 (1995) 515–520, https://doi.org/10.1006/jcis.1995.1353.
[21] J. Cieśla, Z. Sokołowska, B. Witkowska-Walczak, K. Skic, Adsorption of water vapour and the specific surface area of arctic zone soils (Spitsbergen), Int. Agrophys. 32 (2018) 19–27, https://doi.org/10.1515/intag-2016-0076.
[22] H.-T. Oh, S.-J. Lim, J.H. Kim, C.-H. Lee, Adsorption equilibria of water vapor on an alumina/zeolite 13X composite and silica gel, J. Chem. Eng. Data 62 (2017) 804–811, https://doi.org/10.1021/acs.jced.6b00850.
[23] a L. Myers, J.M. Prausnitz, Thermodynamics of mixed-gas adsorption, AIChE J. 11 (1965) 121–127, https://doi.org/10.1002/aic.690110125.
[24] M.M.J. Treacy, J.B. Higgins, Collection of Simulated XRD Powder Patterns for Zeolites, Elsevier, 2007, https://doi.org/10.1016/B978-0-444-53067-7.X5470-7.
[25] C. Kosanović, B. Subotić, I. Šmit, A. Čižmek, M. Stubičar, A. Tonejc, Study of structural transformations in potassium-exchanged zeolite a induced by thermal and mechanochemical treatments, J. Mater. Sci. 32 (1997) 73–78, https://doi.org/10.1023/A:1018514929882.
[26] V. Dondur, N. Petranović, R. Dimitrijevic, High temperature phase transformations of cation exchanged zeolites: a new route for synthesis of aluminosilicate materials, Mater. Sci. Forum 214 (1996) 91–98, https://doi.org/10.4028/www.scientific.net/MSF.214.91.
[27] G.N. Greaves, F. Meneau, A. Sapelkin, L.M. Colyer, I. ap Gwynn, S. Wade, G. Sankar, The rheology of collapsing zeolites amorphized by temperature and pressure, Nat. Mater. 2 (2003) 622–629, https://doi.org/10.1038/nmat963.

[28] J. Gulín-González, G.B. Suffritti, Amorphization of calcined LTA zeolites at high pressure: A computational study, Microporous Mesoporous Mater. 69 (2004) 127–134, https://doi.org/10.1016/j.micromeso.2004.02.002.
[29] Y. Huang, E.A. Havenga, Why do zeolites with LTA structure undergo reversible amorphization under pressure? Chem. Phys. Lett. 345 (2001) 65–71, https://doi.org/10.1016/S0009-2614(01)00856-9.
[30] S. Evans, Correction for the effects of adventitious carbon overlayers in quantitative XPS analysis, Surf. Interface Anal. 25 (1997) 924–930, https://doi.org/10.1002/(SICI)1096-9918(199711)25:12<924::AID-SIA317>3.0.CO;2-2.
[31] T.L. Barr, S. Seal, Nature of the use of adventitious carbon as a binding energy standard, J. Vac. Sci. Technol. A: Vac., Surf., Films 13 (1995) 1239–1246, https://doi.org/10.1116/1.579868.
[32] M. Guisnet, P. Magnoux, D. Martin, Roles of acidity and pore structure in the deactivation of zeolites by carbonaceous deposits, in: 1997: pp. 1–19. https://doi.org/10.1016/S0167–2991(97)80138–3.
[33] S.R. Bare, A. Knop-Gericke, D. Teschner, M. Hävacker, R. Blume, T. Rocha, R. Schlögl, A.S.Y. Chan, N. Blackwell, M.E. Charochak, R. ter Veen, H. H. Brongersma, Surface analysis of zeolites: An XPS, variable kinetic energy XPS, and low energy ion scattering study, Surf. Sci. 648 (2016) 376–382, https://doi.org/10.1016/j.susc.2015.10.048.
[34] C.D. Wagner, W.M. Riggs, L.E. Davis, J.F. Moulder, G.E. Muilenberg, Handbook of X-ray photoelectron spectroscopy, perkin-elmer corporation, Phys. Eletronics Div., Eden Prairie, Minn. (1979).
[35] C. Liu, G. Li, E.J.M. Hensen, E.A. Pidko, Nature and catalytic role of extraframework aluminum in faujasite zeolite: a theoretical perspective, ACS Catal. 5 (2015) 7024–7033, https://doi.org/10.1021/acscatal.5b02268.
[36] J.C.M. Muller, G. Hakvoort, J.C. Jansen, DSC and TG study of water adsorption and desorption on zeolite NaA, J. Therm. Anal. 53 (1998) 449–466, https://doi.org/10.1023/A:1010137307816.
[37] J.W. Park, G. Seo, IR study on methanol-to-olefin reaction over zeolites with different pore structures and acidities, Appl. Catal. A Gen. 356 (2009) 180–188, https://doi.org/10.1016/j.apcata.2009.01.001.
[38] S.M.P. de Lucena, J.C.A. Oliveira, D.V. Gonçalves, L.M.O. Lucas, P.A.S. Moura, R. G. Santiago, D.C.S. Azevedo, M. Bastos-Neto, LTA Zeolite Characterization Based on Pore Type Distribution, Ind. Eng. Chem. Res 61 (2022) 2268–2279, https://doi.org/10.1021/acs.iecr.1c04897.
[39] J. García-Martínez, D. Cazorla-Amorós, A. Linares-Solano, Further evidences of the usefulness of CO_2 adsorption to characterize microporous solids. : Encycl. Volcano (2000) 485–494, https://doi.org/10.1016/S0167-2991(00)80054-3.
[40] S. Brunauer, P.H. Emmett, E. Teller, Adsorption of gases in multimolecular layers, J. Am. Chem. Soc. 60 (1938) 309–319, https://doi.org/10.1021/ja01269a023.
[41] G. Busca, Acidity and basicity of zeolites: a fundamental approach, Microporous Mesoporous Mater. 254 (2017) 3–16, https://doi.org/10.1016/j.micromeso.2017.04.007.
[42] P. Nachtigall, M.R. Delgado, D. Nachtigallova, C.O. Arean, The nature of cationic adsorption sites in alkaline zeolites — single, dual and multiple cation sites, (2012) 1552–1569. https://doi.org/10.1039/c2cp23237e.
[43] S.H. Shim, A. Navrotsky, T.R. Gaffney, J.E. Macdougall, Chabazite: energetics of hydration, enthalpy of formation, and effect of cations on stability, Am. Mineral. 84 (1999) 1870–1882, https://doi.org/10.2138/am-1999-11-1214.
[44] T. Kawai, K. Tsutsumi, Evaluation of hydrophilic-hydrophobic character of zeolites by measurements of their immersional heats in water, Colloid Polym. Sci. 270 (1992) 711–715, https://doi.org/10.1007/BF00654048.